Nov 5th, 12:00 AM - 12:00 AM

Experimental Investigation on Ultimate Capacity of Eccentrically-Compressed Cold-Formed Beam-Columns with Lipped Channel Sections

Yuanqi Li

Yinglei Li

Yanyong Song

Twenty-Second International Specialty Conference on Cold-Formed Steel Structures
St. Louis, Missouri, USA, November 5 & 6, 2014

Experimental investigation on ultimate capacity of eccentrically-compressed cold-formed beam-columns with lipped channel sections

Yuanqi Li[1], Yinglei Li[2] and Yanyong Song[2]

Abstract

This paper is mainly concerned with the in-plane behavior of eccentrically-compressed cold-formed steel beam-columns with lipped channel sections. The tested members are classified into three series by loading types including: axial compression and major axis bending (X), axial compression and minor axis bending (lips in tension, Y1), and axial compression and minor axis bending (lips in compression, Y2). A numerical model is developed and verified by the experimental results. Then the elastic local buckling loads are discussed based on test results, numerical analysis, and design methods. The comparison between test strength and nominal strength obtained by AISI specification indicates that the interaction equation can provide conservative prediction for beam-columns' strength.

Introduction

Cold-formed steel members are widely used in many types of metal structures due to its lightness, high strength and stiffness. The cold-formed steel members which are subject to combined compressive axial load and bending are usually referred to as beam-columns. The bending may result from eccentric loading, transverse loads, or applied moments (Yu 2000). It's convenient to discuss the behavior of beam-columns under the three separate headings of in-plane behavior, flexural-torsional buckling, and biaxial-bending (Trahair et al. 2008).

This paper mainly investigated the in-plane behavior of eccentrically-compressed cold-formed steel beam-columns with lipped channel sections, which are subject to axial compression and major or minor axis bending. Totally 57 eccentrically-compressed beam-columns with varying length and different bending directions were tested, and the test strengths are compared with the design strengths obtained using interaction equations in AISI specification.

[1] Professor, Department of Building Engineering, Tongji University, State Key Laboratory of Disaster Reduction in Civil Engineering, Shanghai 200092, China. E-mail: liyq@ tongji.edu.cn
[2] Graduate student, Department of Building Engineering, Tongji University, Shanghai 200092, China.

Literature review

Currently, there are two types of design methods for cold-formed steel members: Effective Width Method (EWM), which is adopted in design codes worldwide, and Direct Strength Method (DSM). DSM is rapidly gaining acceptance as a reliable and efficient method and has been adopted by the codes in North America (2007) and Australia/New Zealand (2005).

Rodrigo and Dinar (Rodrigo and Dinar 2004) conducted the investigation on dealing with the application of beam-column interaction formulae in European Code to isolated steel members with arbitrary loading and end support conditions. Mohri et al. (Mohri et al. 2008) established closed-form solutions for lateral buckling loads of thin-walled, I-section beam-columns under combined axial and bending loads. Hasham and Rasmussen (Hasham and Rasmussen 1998) conducted a series tests on short thin-walled, welded I-sections beam-columns. The test strengths are compared with the design strengths predicted by specifications to assess the accuracy of existing design interaction curves. Teng et al. (Teng et al. 2003) proposed a closed-form solution, whose results match well with finite strip prediction, for distortional buckling mode of cold-formed channel sections subject to combined compression and biaxial bending. Li (Li 2002) conducted totally 55 beam-column tests on cold-formed lipped channel sections to validate the North American design code. The tests included pure compression and pure bending tests, as well as tests with varying ratios of axial-force to major axis bending moment.

Experimental investigation

Material properties

Tensile coupon tests were carried out in accordance with *Metallic Materials – Tensile Testing at Ambient Temperature* (GB/T 228-2002)(2002) to determine the material properties, including yield stress (F_y), tensile strength (F_u), elongation ratio (R_e), and Modulus of elasticity (E). The steel grade of the tested members is S280, with nominal yield stress of 280MPa. As tested sections were pressed from two lots of steel sheets, two groups of material properties were obtained through coupon tests. The test results are summarized in Table 1.

Table 1 Material properties

No.	Specimen	t (mm)	F_y (Mpa)	F_u (Mpa)	R_e (%)	E ($\times 10^5$MPa)
1	S10-1	1.00	303.4	365.0	39.2	1.9
	S10-2	1.00	305.8	365.1	42.3	1.9
	S10-3	1.00	308.1	370.2	38.8	1.9
	S10-4	1.00	310.1	363.9	36.9	2.3
	Avg.	1.00	306.9	366.1	39.3	2.0
2	S10-5	1.00	312.1	359.2	39.4	2.0
	S10-6	1.00	316.1	365.6	40.9	1.9
	S10-7	1.00	332.4	385.7	40.7	2.1

S10-8	1.00	302.5	355.3	39.3	2.2
S10-9	1.00	334.0	385.3	37.7	1.6
Avg.	1.00	319.4	370.2	39.6	2.0

Test specimens

Specimens tested in this investigation were constructed of two kinds of lipped channel sections, which are donated with SEC89 and SEC140. Fig. 1 illustrates the cross-section used in this study.

Based on loading types, the specimens are classified into three series: (1) axial compression and major axis bending (donated as X); (2) axial compression and minor axis bending (lips in tension, donated as Y1); (3) axial compression and minor axis bending (lips in compression, donated as Y2). Sections' nominal dimensions are summarized in Table 2 and members' nominal length ranges from 600mm to 2400mm. The dimensions of tested specimens were recorded at the mid-length and each end of the specimen for a total of three measurement locations. The labeling rule of specimens is shown in Fig. 2.

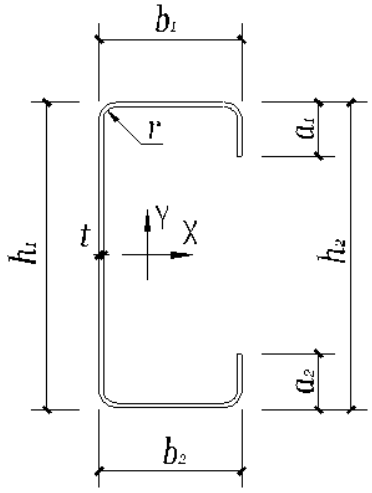

Fig. 1 Cross section geometry

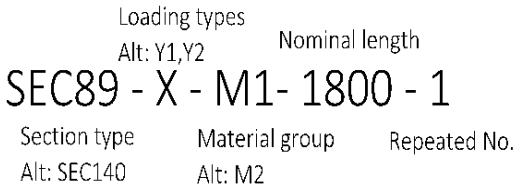

Fig. 2 Labeling rules

Table 2 Nominal dimensions of cross section

Section	h_1 (mm)	h_2 (mm)	b_1 (mm)	b_2 (mm)	a_1 (mm)	a_2 (mm)	r (mm)	t (mm)

SEC89	89	89	41	41	13	13	3.05	1.00
SEC140	140	140	41	41	13	13	3.05	1.00

Test setup

In this experimental investigation, the compressive load and bending moment were achieved by applying eccentric force. Hydraulic jack and reaction frame were used to apply eccentric compressive load on specimens. All the tests were performed in displacement control between pinned ends in a vertical reaction frame.

For members under axial compression and major axis bending, braces were fixed to restrain members' out-of-plane deflection. In order to avoid crippling at members' ends, hoop-plates were applied in the test.

The bidirectional-hinged supports (Li et al. 2010) was adopted to simulate pin-end conditions. As the tests did not involve bi-axial bending, one plate of each support assembly was restrained against rotation to achieve only one direction bending. The calculation length L_0=L+90 mm, where L is specimen's actual length.

Setting the specimen in the test rig is the most important and difficult part of the testing program. Each specimen should be placed at a particular distance (i.e. eccentricity, donated as e in Table 6) to the load point along major or minor axis. After the geometric alignment was completed, approximately 10% load of predicted ultimate capacity was applied on the specimen. Based on the cross-section's stress distribution acquired by strain gauges, the actual eccentricity was calculated and specimen's location was adjusted to achieve the target eccentricity. This procedure was called physical alignment. After finishing geometric and physical alignment, the eccentric load was applied until the load dropped below 80% of the tested peak load.

Test results

The averaged failure load, P_t, was the largest load that each member sustained during a test. Table 6 summarized the failure loads.

Members under axial compression and major axis bending displayed two kinds of failure modes: one was flange's inward rotation followed by web's local buckling, and the other was web local buckling followed by flange's inward rotation (Fig. 3). Members with slenderness ratio less than 25 still kept straight after failure. Besides this, members' failure locations were diverse, including middle part, ends and the location where the braced were fixed.

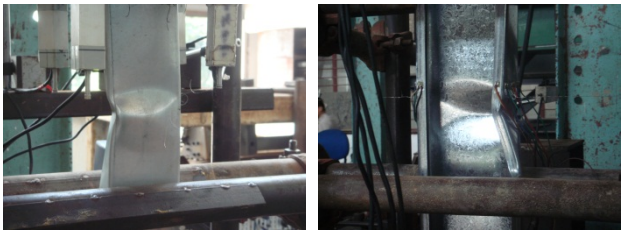

Fig. 3 Failure modes for beam-columns under axial compression and major axis bending

For members under axial compression and minor axis bending (lips in tension), as the load increased, web's local buckling, followed by flanges' deformation, was observed (Fig. 4). The phenomenon of overall bending in single curvature was obvious for members with large slenderness ratios. All the members' failure occurred at the middle part.

For members under axial compression and minor axis bending (lips in compression), as the load increased, the flanges' inward or outward rotation occurred abruptly, which displayed I-I or O-O distortional failure mode (Fig. 5). Compared to the previous loading type with load acting eccentric to web, this kind of beam-column's load-displacement curve showed a more "brittle" failure. The web's local buckling was not observed during the test.

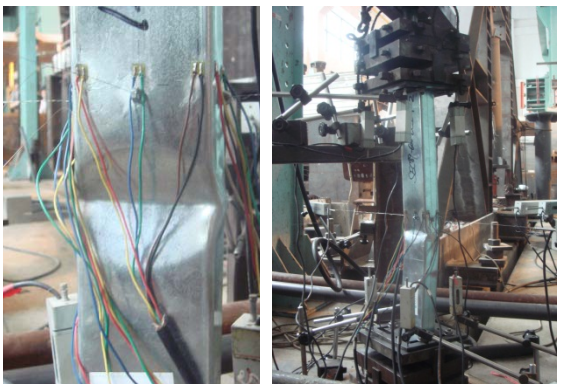

Fig. 4 Failure modes for beam-columns under axial compression and minor axis bending (lips in tension)

Fig. 5 Failure modes for beam-columns under axial compression and minor axis bending (lips in compression)

Finite element analysis

The commercial finite element package ANSYS12.0 was used for both elastic buckling and nonlinear collapse analysis of cold-formed steel

beam-columns in this research. The finite element model was verified by test results.

Element type and mesh density

Since the material thickness of cold-formed steel members is thin compared to the element's width, the shell element is an appropriate choice. SHELL181, which is a 4-node element with six degrees of freedom at each node, was adopted to simulate specimens and the elastic element SHELL63 was used for end support plates.

The effect of mesh density is studied in this paper. Two kinds of element size (2mm×4mm and 5mm×10mm) are employed in the ANSYS models and the analysis results are summarized in Table 3. The comparison indicates that the 5mm×10mm element size is suitable for the analysis.

Material modelling

Material nonlinearity is a consideration for nonlinear collapse analysis of cold-formed steel members. The engineering stress-strain (σ_e-ε_e) curve had been obtained through coupon tensile tests. The true stress-strain (σ_{true}-ε_{true}) employed in ANSYS should be converted from engineering stress-strain by equation (1) and (2).

$$\sigma_{true} = \sigma_e(1+\varepsilon_e) \tag{1}$$

$$\varepsilon_{true} = \ln(1+\varepsilon_e) \tag{2}$$

As all the components of the tests were made of steel, the Poisson's ratio is set to 0.3 and Modulus of elasticity (E) is set to 2.0×10^5MPa in according with the coupon tensile test results. Since the end supports were composed of thick plates and were of little interest in this research, they were modeled as rigid bodies by setting an artificially high E=2.0×10^7MPa.

Boundary conditions

In the experimental investigation, the bidirectional-hinged supports (the rotation in one direction was restrained) were applied to achieve pin-end supporting conditions. A simplified model was adopted in ANSYS to simulate the end supports. For members under axial compression and major axis bending, the nodes on the web-flange juncture, where the braces were fixed in the tests, were restrained against out-of plane deflection.

Geometric imperfection

Thin-walled members' strength is sensitive to the geometric imperfection. In this paper, the geometric imperfection was divided into three categories: global imperfection (Fig. 6a), local imperfection (Fig. 6b) and distortional imperfection (Fig. 6c). The local imperfection was derived from Eigen-buckling analysis. A combination of the first three local buckling modes was introduced into perfect models, while the global and distortional imperfections were seeded by conducting a limit-load analysis on the model.

The magnitude of the imperfection is also important in the analysis. In this research, the imperfection was not measured due to the lack of appropriate and efficient measuring devices. The global imperfection magnitude is commonly taken as δ_G=L/1000, where L is member's length. The magnitude of the local and distortional imperfections was determined based on statistical data summarized by Zeinoddini and Schafer (Zeinoddini and Schafer 2012). The local and distortional imperfection values are set to δ_L=0.31t and δ_D=0.75t (t is plate's thickness) respectively, which are corresponding to 50% probability of exceedance.

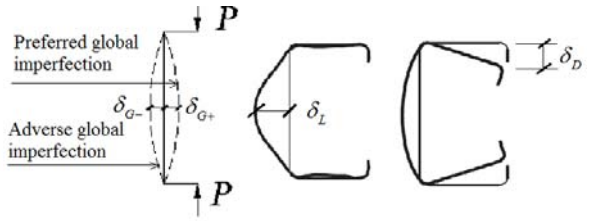

(a) global (b) local (c) distortional
Fig. 6 Geometric imperfection types

For beam-columns under axial compression and bending, the sign of global imperfection could greatly influence members' ultimate capacity. As shown in Fig. 6a, the global imperfection could be classified into preferred imperfection (donated as G+) and adverse imperfection (donated as G-). The analysis results for these two kinds of global imperfection are summarized in Table 3.

Solution method

For Eigen-buckling analysis, the Lanczos method is adopted, while for nonlinear collapse analysis, Newton-Raphson method with displacement control is employed.

It's should be noted that the residual stress and cold-work effect are not considered in this paper.

Analysis results

The ANSYS analysis results are reported in Table 3, including Eigen-buckling loads (P_{cr}), nonlinear collapse analysis results (P_u), and averaged tested failure loads (P_{t_ave}). In the table, G- stands for adverse global imperfection, G+ stands for preferred global imperfection, 2mm×4mm (or 5mm×10mm) stands for element size.

The results comparison between ANSYS model with 2mm×4mm and 5mm×10mm element indicates that refine the mesh from 5mm×10mm to 2mm×4mm could not increase the analysis precision obviously, so in this paper the element size is set to 5mm×10mm to save the computing time.

Table 3 shows that: for members under compression and major axis bending, the ANSYS analysis results of models seeded with adverse global imperfection were more closely to members' tested failure loads, while the preferred imperfection model is more suitable for members under axial compression and minor axis bending.

Table 3 ANSYS analysis results

Specimen	P_t (kN)	P_{cr} (kN)	G- 2×4 P_u/P_{t_ave}	G- 5×10 P_u/P_{t_ave}	G+ 5×10 P_u/P_{t_ave}
SEC89-X-M2-600	34.5	26.7	0.93	0.94	0.97
SEC89-X-M1-900	31.4	26.5	0.99	1.00	1.04
SEC89-X-M1-1200	31.3	26.4	0.97	0.97	1.01
SEC89-X-M2-1200	31.2	26.4	1.01	1.01	1.05
SEC89-X-M2-1500	30.9	26.4	0.98	0.99	1.04

SEC89-X-M1-1800	31.4	26.4	0.91	0.92	0.98
SEC89-X-M2-1800	30.1	26.4	0.99	0.99	1.05
SEC140-X-M2-600	34.9	14.4	0.99	1.00	1.02
SEC140-X-M2-900	35.1	14.1	0.97	0.98	1.01
SEC140-X-M2-1200	33.1	14.0	1.04	1.04	1.06
SEC140-X-M2-1500	31.7	14.0	1.05	1.06	1.08
SEC140-X-M2-1800	31.0	14.0	1.07	1.08	1.12
SEC140-X-M2-2400	30.6	13.9	1.05	1.05	1.11
Avg.			1.00	**1.00**	1.04
Stdev.			0.05	**0.04**	0.04
SEC89-Y1-M2-600	29.2	18.7	0.88	0.89	0.93
SEC89-Y1-M1-1200	22.8	18.7	0.88	0.88	0.96
SEC89-Y1-M1-1800	16.6	18.7	0.89	0.89	0.98
SEC140-Y1-M2-1200	20.8	10.9	1.01	1.02	1.09
SEC140-Y1-M2-1800	15.9	10.9	0.96	0.97	1.05
Avg.			0.93	0.93	**1.00**
Stdev.			0.05	0.05	**0.06**
SEC89-Y2-M2-600	32.0	43.8	0.95	0.95	1.01
SEC89-Y2-M1-1200	27.2	43.8	0.82	0.82	0.90
SEC89-Y2-M1-1800	19.6	29.4	0.82	0.83	0.95
SEC140-Y2-M2-1200	26.1	20.4	0.97	0.96	1.04
SEC140-Y2-M2-1800	20.3	20.3	0.89	0.88	1.00
Avg.			0.89	0.89	**0.98**
Stdev.			0.06	0.06	**0.05**

Experimental results analysis

Elastic local buckling loads

The experimental elastic local buckling loads (P_{tcrl}) were determined based on the load-strain curves at members' mid-length. It is assumed that the P_{tcrl} is the load at which the strain reaches the maximum (Venkataramaiah and Roorda 1982). Members' elastic local buckling loads are summarized in Table 4.

Table 4 Elastic local buckling loads of beam-columns

Specimen	P_{tcrl} (kN)	Specimen	P_{tcrl} (kN)
Axial compression and major axis bending (X)		Axial compression and minor axis bending (lips in tension, Y1)	
SEC89-X-M2-600-1	22.1	SEC89-Y1-M2-600-1	17.4
SEC89-X-M2-600-2	21.9	SEC89-Y1-M2-600-2	18.6
SEC89-X-M2-1200-1	21.7	SEC89-Y1-M1-1200-1	16.8

SEC89-X-M2-1500-3	20.8	SEC89-Y1-M1-1800-1	13.2
SEC140-X-M2-600-2	19.0	SEC89-Y1-M1-1800-2	14.4
SEC140-X-M2-600-3	16.9	SEC140-Y1-M2-1200-2	8.1
SEC140-X-M2-900-1	11.1	SEC140-Y1-M2-1800-1	8.2
SEC140-X-M2-900-2	11.8	SEC140-Y1-M2-1800-3	8.2
SEC140-X-M2-1200-1	10.0		
SEC140-X-M2-1200-2	10.4		
SEC140-X-M2-1200-3	11.0		
SEC140-X-M2-1500-1	10.4		
SEC140-X-M2-1500-3	10.1		
SEC140-X-M2-1800-2	9.7		
SEC140-X-M2-1800-4	12.3		
SEC140-X-M2-2400-1	10.9		

Several conclusions can be made from the load-strain curves and members' elastic local buckling loads: (a) after elastic local buckling occurs, member can still keep bearing the loads for a long time, which exhibits significant post-buckling behavior; (b) for members under axial compression and major axis bending, load-strain curves indicate web's local buckling happens before flanges'; (c) the elastic distortional buckling loads can't be obtained from the load-strain curves; (d) as members' length increases, the elastic local buckling load decreases in small amplitude (generally less than 10%). This may be caused by the fact that Second-order effect is not obvious for the tested members at this load level.

A comparison between the experimental elastic local buckling loads (P_{tcrl}), ANSYS Eigen-buckling results (P_{Acrl}), and CUFSM (Li and Schafer 2010) buckling analysis results (P_{Ccrl}) was conducted for short members (Table 5). The CUFSM loads are in well agreement with ANSYS results, which shows that CUFSM can provide precise prediction on the local buckling loads. However, the discreteness of tested loads are serious, this may be partly due to the difficulty to precisely predict the location where the local buckling firstly occurs and the influence of imperfection.

Table 5 Comparison of elastic local buckling loads

Specimen	P_{Ccrl} (kN)	P_{Acrl} (kN)	P_{tcrl} (kN)
SEC89-X-M2-600-1	27.0	26.7	22.1
SEC89-Y1-M2-600-2	19.0	18.7	18.6
SEC89-Y2-M2-600-1	42.5	43.8	-
SEC140-X-M2-600-3	14.2	14.4	16.9
SEC140-Y1-M2-1200-2	11.7	10.9	8.1
SEC140-Y2-M2-1200-1	18.2	20.4	-

Comparison between experimental strength and design strength

The tested beam-columns' strengths (donated as P) are determined according to AISI specification. This design approach is to calculate

member's ultimate capacities corresponding to axial compression and pure bending, and then to stipulate a linear interaction curve that connects the limiting case for any combination of axial force and bending moment.

In this paper, the resistance factors (ϕ_c, ϕ_b), and moment gradient factor (C_{mx} or C_{my}) are set to 1.0. The nominal axial strength (P_n) and nominal flexural strength (M_n) are determined using effective width method (EWM) and direct strength method (DSM). It should be noted that member's nominal strength is calculated based on initiation of yielding except for members bending about minor axis (web in compression), whose flexural strength is determined based on inelastic reserve capacity.

In order to validate the accuracy of the linear interaction equation without the influence of inaccuracy when determining P_n and M_n using current design provisions, each beam-column's axial strength and pure bending strength are obtained by ANSYS analysis.

All the members' predicted strengths using different methods (including ANSYS method, EWM, and DSM) and tested strength (P_t) are reported in Table 6.

The comparison between ANSYS results and tested failure loads indicates that the linear interaction equation is appropriate for beam-column under combined axial compression and major axis bending or under combined axial compression and minor axis bending (lips in tension). However, for beam-columns under axil compression and minor axis bending (lips in compression), the predicted strength is averaged 76% times of the tested strength with standard deviation 0.03. This conservative prediction may be caused by the fact that the shift of effective centroid reduces the load eccentricity (Young and Rasmussen 1999). Generally speaking, the design provision provides conservative prediction for beam-columns' ultimate capacity mainly due to the conservative prediction of members' axial compression strength and bending strengths. The EWM results match better with test results than DSM.

Conclusions

In this paper, Totally 57 eccentrically-compressed beam-columns are tested and their in-plane structural behaviors are discussed by experimental investigation and numerical analysis. The test results are compared with nominal strength predicted by design specifications. Several conclusions can be summarized as following:

(1) The ANSYS model with carefully attention on material model and geometric imperfection can predict beam-column's strength accurately.

(2) The experimental investigation indicates that using CUFSM to get beam-column's elastic local buckling load is reliable.

(3) The interaction equation method, which is commonly adopted in design specifications worldwide, can predict beam-column's strength reliably but a little conservatively. Nevertheless, some shortcomings of this method are obvious and more improvements are still needed.

Acknowledgements

Authors are grateful to the financial support by the National Natural Science Foundation of China (No. 51078288).

References

GB/T 228-2002. (2002). Metallic Materials – Tensile Testing at Ambient Temperature, Beijing.
AS/NZS,AS/NZSNo.4600:2005. (2005). Cold-Formed Steel Structures, Sydney.
AISI-S100-07. (2007). North American Specification for the Design of Cold-Formed Steel Structural Members, Washington.
Hasham, A. S., and Rasmussen, K. J. R. (1998). "Section Capacity of Thin-Walled I-Section Beam-Columns." *Journal of Structural Engineering*, 124(4), 351-359.
Li, L. (2002). "Strength of Cold-Formed Steel Beam-Columns,", McMaster University, Hamilton.
Li, Y., Wang, S., Shen, Z., and Yao, X. (2010). "Experimental Study and Load-Carrying Capacity Analysis of High-Strength Cold-Formed Thin-Walled Steel Lipped Channel Columns under Axial Compression." *Journal of Building Structures*, 31(11), 17-25.
Li, Z., and Schafer, B. W. (2010). "Application of the Finite Strip Method in Cold-Formed Steel Member Design." *Journal of Constructional Steel Research*, 66, 971-980.
Mohri, F., Bouzerira, C., and Potier-Ferry, M. (2008). "Lateral Buckling of Thin-Walled Beam-Column Elements under Combined Axial and Bending Loads." *Thin-Walled Structures*, 46(3), 290-302.
Rodrigo, G., and Dinar, C. (2004). "On the Application of Beam-Column Interaction Formulae to Steel Members with Arbitrary Loading and Support Conditions." *Journal of Constructional Steel Research*, 60, 433-450.
Teng, J. G., Yao, J., and Zhao, Y. (2003). "Distortional Buckling of Channel Beam-Columns." *Thin-Walled Structures*, 41(7), 595-617.
Trahair, N. S., Bradford, M. A., Nethercot, D. A., and Gardner, L. (2008). *The Behaviour and Design of Steel Structures to EC3*, Taylor & Francis, New York.
Venkataramaiah, K. R., and Roorda, J. (1982). "Analysis of Local Plate Buckling Experimental Data." 6th International Specialty Conference on Cold-Formed Steel Structures, St. Louis, 45-74.
Young, B., and Rasmussen, K. J. R. (1999). "Shift of Effective Centroid of Channel Columns." *Journal of Structural Engineering*, 125(5), 524-531.
Yu, W. (2000). *Cold-Formed Steel Design*, John Wiley & Sons, Inc., New York.
Zeinoddini, V. M., and Schafer, B. W. (2012). "Simulation of Geometric Imperfections in Cold-formed Steel Members Using Spectral Representation Approach." *Thin-Walled Structures*, 60, 105-117.

Table 6 Comparison of beam-columns' test strength and predicted strength

Specimen	e (mm)	P_t (kN)	ANSYS				EWM				DSM			
			P_n (kN)	M_n (kNm)	P (kN)	P/P_t	P_n (kN)	M_n (kNm)	P (kN)	P/P_t	P_n (kN)	M_n (kNm)	P (kN)	P/P_t
SEC89-X-M2-600	17.75	34.5	46.1	1.80	31.4	0.91	45.5	1.68	30.5	0.88	39.5	1.68	27.7	0.80
SEC89-X-M1-900	17.75	31.4	44.8	1.77	30.3	0.97	44.5	1.64	29.5	0.94	37.9	1.64	26.5	0.84
SEC89-X-M1-1200	17.75	31.3	44.0	1.77	29.5	0.94	43.7	1.64	28.7	0.92	37.1	1.64	25.8	0.82
SEC89-X-M2-1200	17.75	31.2	45.6	1.83	30.6	0.98	44.8	1.68	29.4	0.94	38.0	1.68	26.4	0.85
SEC89-X-M2-1500	17.75	30.9	44.4	1.84	29.6	0.96	43.3	1.68	28.3	0.92	36.9	1.68	25.5	0.83
SEC89-X-M1-1800	17.75	31.4	42.6	1.78	27.9	0.89	40.6	1.64	26.4	0.84	34.9	1.64	24.0	0.77
SEC89-X-M2-1800	17.75	30.1	44.1	1.85	28.8	0.96	41.6	1.68	27.0	0.90	35.6	1.68	24.5	0.81
SEC140-X-M2-600	26.74	34.9	48.3	3.10	34.0	0.97	41.5	2.77	29.6	0.85	36.7	2.75	27.0	0.77
SEC140-X-M2-900	26.74	35.1	46.8	3.20	33.5	0.95	41.5	2.77	29.5	0.84	36.4	2.75	26.7	0.76
SEC140-X-M2-1200	26.74	33.1	46.8	3.19	33.3	1.01	41.5	2.77	29.4	0.89	36.0	2.75	26.5	0.80
SEC140-X-M2-1500	26.74	31.7	46.0	3.19	32.7	1.03	41.5	2.77	29.2	0.92	35.6	2.75	26.1	0.82
SEC140-X-M2-1800	26.74	31.0	46.1	3.21	32.5	1.05	41.5	2.77	29.0	0.94	35.0	2.75	25.7	0.83
SEC140-X-M2-2400	26.74	30.6	45.5	3.21	31.6	1.03	41.5	2.77	28.5	0.93	33.7	2.75	24.7	0.81
Avg.						0.97				0.90				0.81
Stdev.						0.05				0.04				0.03
SEC89-Y1-M2-600	7.74	29.2	38.2	0.71	26.0	0.89	43.2	0.73	28.4	0.97	36.4	0.57	23.4	0.80
SEC89-Y1-M1-1200	7.74	22.8	33.5	0.69	21.5	0.94	33.8	0.71	21.8	0.96	29.7	0.55	18.8	0.82
SEC89-Y1-M1-1800	7.74	16.6	24.5	0.67	16.1	0.97	22.5	0.71	15.4	0.93	22.1	0.55	14.3	0.86
SEC140-Y1-M2-1200	7.38	20.8	31.1	0.76	21.9	1.05	34.6	0.76	23.3	1.12	28.2	0.50	18.3	0.88

SEC140-Y1-M2-1800	7.38	15.9	21.9	0.73	15.8	0.99	22.1	0.76	16.0	1.01	20.3	0.50	13.8	0.87
Avg.						0.97				1.00				0.85
Stdev.						0.05				0.07				0.03
SEC89-Y2-M2-600	7.74	32.0	38.3	0.62	24.9	0.78	43.2	0.57	26.1	0.82	36.5	0.59	23.7	0.74
SEC89-Y2-M1-1200	7.74	27.2	33.6	0.59	20.6	0.76	33.9	0.55	20.2	0.74	29.8	0.57	19.0	0.70
SEC89-Y2-M1-1800	7.74	19.6	24.8	0.59	15.7	0.80	22.6	0.55	14.6	0.74	22.2	0.57	14.5	0.74
SEC140-Y2-M2-1200	7.38	26.1	29.6	0.60	19.8	0.76	33.4	0.56	20.8	0.80	26.8	0.60	18.6	0.71
SEC140-Y2-M2-1800	7.38	20.3	21.1	0.60	14.7	0.72	21.3	0.56	14.5	0.72	19.3	0.60	13.9	0.69
Avg.						0.76				0.76				0.72
Stdev.						0.03				0.04				0.02